Time-varying tool influence function model of bonnet polishing for aspheric surfaces

Bo Zhong,[1,*] Chunjin Wang,[2] Xianhua Chen,[1] Jian Wang,[1]

[1] *Research Center of Laser Fusion, China Academy of Engineering Physics, Mianyang 621900, China*

[2]*Department of Industrial and Systems Engineerin, The Hong Kong Polytechnic University, Hung Hom, Kowloon, Hong Kong, China*

**Corresponding author: zhongbo_foerc@163.com*

Received XX Month XXXX; revised XX Month, XXXX; accepted XX Month XXXX; posted XX Month XXXX (Doc. ID XXXXX); published XX Month XXXX

In the actual process, the tool influence function (TIF) is time-varying, induced by the different surface curvature on aspheric surface. Consequently, this paper carried out the investigation on the surface curvature effect to the bonnet-workpiece contact area, and presented a time-varying TIF modeling method. Time-varying TIF was modelled based on the finite element analysis and kinematics analysis methods, and validated by experiments. The experimental results exhibited good agreement with the theoretical results. This model can forecast the TIF for different polishing positions on aspheric surfaces and provide the theoretical foundation for dynamic compensation polishing of aspheric surface.© 2018 Optical Society of America

OCIS codes: *(240.0240) Optics at surfaces; (240.5450) Polishing.*

http://dx.doi.org/10.1364/AO.99.099999

Symbols

C_1, C_2, C_3	contact area	ρ	precession angle
D_p	polar distance	R_1	bonnet radius
R_c	nearest spherical radius of the sub-region under different polar distance or spherical radius of sphere workpiece	h	height of the workpiece in the contact area
		r	radius of the contact area
R_0	vertex curvature radius	O	bonnet center
k	conic coefficient	O_1	intersection of the spindle axis and the contact interface
$R_{TIF}(x,y)$	the average material removal per unit time	O_2	center of the contact area
K	Preston coefficient	ω	bonnet rotational speed
V	velocity distribution	p	an arbitrary point on the workpiece in the contact area
P	pressure distribution	p_1	the projection of point p on the axis of the bonnet spindle
T	polishing time	PRR	peak removal rate
m	shape factor	VRR	volume removal rate
A	maximum contact pressure value in the contact area	D_x	the distance between the polar center and the geometrical center of the aspheric surface in the X direction
B	half-length of the elliptical contact area		
C	half-width of the elliptical contact area	D_y	the distance between the polar center and the geometrical center of the aspheric surface in the Y direction
H	tool compression		
$RMSE$	root mean square of the error between the fitting data and the original data	PV	peak value
		Z_{actual}	experimental TIF

1. INTRODUCTION

Bonnet polishing technology has been successfully used in precision polishing of freeform surfaces, such as aspheric optics, optical molds, freeform artificial joint, etc. [1-4], depending on its adaptability to freeform surface and high polishing efficiency. During polishing, its material removal is generated based on the convolution between tool influence function (TIF) and the dwell time [5]. Hence, precision TIF model is critical for simulation and prediction of material removal in bonnet polishing.

Viewing this, several researchers carried out the studies on the modeling of TIF. Kim et al. [6] proposed a reverse-computation technique that traces the real polishing pressure from the empirical TIF. Li et al. [7] presented a simulation technique to predict TIF based on the precessions polishing process, and the simulation results of TIFs are verified by an experiment that shows the residual errors are less than 5%. Wang et al. [8,9] investigated the model of the static tool influence function (sTIF) of bonnet polishing (BP), and a group of experiments to extract the polishing spots were conducted to verify the accuracy of the sTIF model. Zeng et al. [10] reported a modified Preston equation model combining process parameters to allow prediction of the material removal rate during bonnet polishing. Cao et al. [11] presented a multi-scale theoretical model for the prediction and simulation of the material removal characteristics in BP process. Pan et al. [12] indicated that modification of TIF of bonnet polishing based on interfacial friction coefficient can improve the modeling accuracy. Within these modeling method, the TIF is considered to be constant during polishing process.

However, there exists material removal rate variance during practical bonnet polishing of aspheric surfaces, induced by the variance of the surface curvature [13], and little attention has been paid to the TIF modeling considering the curvature effect during bonnet polishing aspheric surfaces. Recently, Song et al. [14] pointed out the curvature effect in bonnet polishing of aspheric surface, and present the maximum material removal depth and surface roughness prediction models. But the TIF model of BP considering the curvature effect still has not been developed. Hence, a 3D time-varying TIF modeling method was developed in this paper aiming to provide a precision TIF model considering curvature effect during bonnet polishing of aspheric surfaces.

2. SURFACE CURVATURE EFFECT DURING BONNET POLISHING OF ASHERIC SURFACE

2.1. The effect of surface curvature to the bonnet-workpiece contact area

According to Fig. 1(a), there is a significant difference in the contact area between the bonnet and workpiece with different curvature under the same compression. The contact areas of the bonnet and the convex surface, the plane surface, and the concave surface respectively correspond to the contact areas C_1, C_2, and C_3, and their size in descending order are as follows: C_3, C_2, and C_1. Based on three workpieces, i.e. concave surface with 500mm radius, flat surface, and convex surface with 500mm radius, the contact area between the bonnet and the three workpieces was detected using a static pressure sensor (made by Tekscan) under 0.65mm compression. The test result is shown in Fig.1(b), which has an agreement with the result of Fig. 1(a).

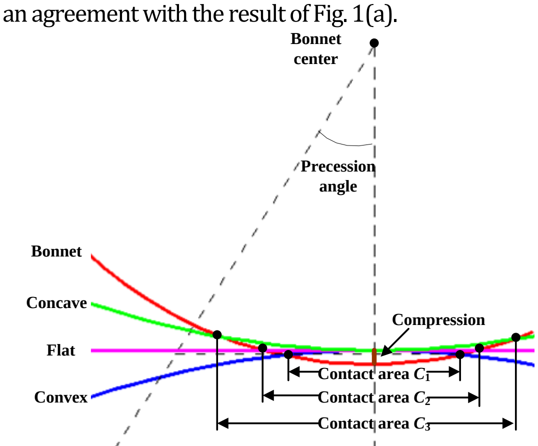

(a)

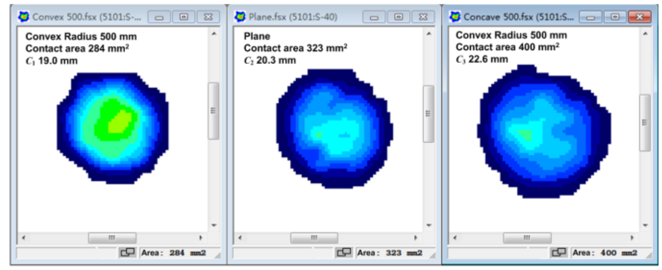

(b)

Fig. 1. Comparison of contact area between bonnet and convex surface, plane surface and concave surface. (a) geometrical result, (b) actual contact test.

2.2. Local curvature radius calculation in the contact area on aspheric surface

In this paper, the local contact area between the bonnet and the aspherical surface is approximated as its closest spherical surface. Therefore, the spherical radius of the contact area when the bonnet moves on the aspherical surface needs to be calculated.

Taking the quadric aspheric surface with the parameters, i.e., the vertex curvature radius R_0 1600 mm, and the conic coefficient k -1, as example, and the analyzed local area size is 50mm. Using the least squares method introduced by the authors [15], the nearest spherical radius (R_c) of the sub-regions under different polar distances (D_p, the distance between the polar center and the sub-region center) is obtained. Fig. 2(a) shows the distribution of the R_0 for each sub-region. Fig. 2 (b) shows the relationship between the polar distance and the nearest spherical radius.

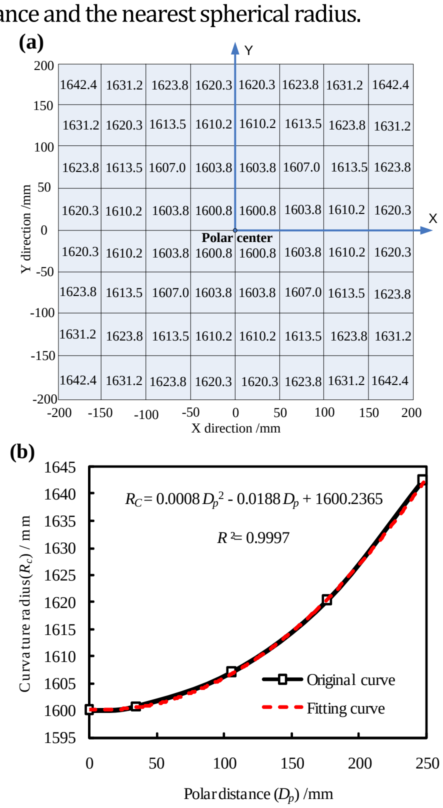

Fig. 2. (a) The distribution of the nearest spherical radius for each sub-region, (b) the relationship between the polar distance and the nearest spherical radius.

As can be seen from Fig. 2(b), the greater the polar distance of the local area is, the greater the curvature radius is. When the polar distance is zero, the fitting curvature radius is equal to the vertex curvature radius. And the relationship between the curvature radius R_c and the polar distance D_p is:

$$R_c = f_{Rc}(D_p) = 0.0008D_p^{\ 2} - 0.0188D_p + 1600.2365 \qquad \textbf{(1)}$$

3. MODELING OF THE TIME-VARYING TOOL INFLUENCE FUNCTION

Under some assumptions, the relation between the material removal of bonnet polishing and various process parameters can be described by the Preston equation. $R_{TIF}(x,y)$ is the average material removal per unit time:

$$R_{TIF}(x,y) = \frac{1}{T}\int_0^T K \cdot P(x,y) \cdot V(x,y)dt \qquad \textbf{(2)}$$

where K is the preston constant, V is the velocity distribution, P is the pressure distribution, T is the polishing time.

In equation (2), pressure distribution P and velocity distribution V are related to the workpiece curvature R_c. Firstly, the contact pressure P and the velocity distribution V related to R_c is solved through the finite element analysis and kinematics analysis of contact states between the bonnet and different curvature workpieces. Then, according to the variation law of the polar distance D_p in the machining process, a time-varying TIF model related to aspherical machining position (or time) can be obtained.

3.1. The effect of surface curvature to the bonnet-workpiece contact area

A. Stress distribution by finite element analysis

The ANSYS analysis model for the contact pressure between bonnet and workpieces with different curvatures is shown in Fig. 3. The bonnet is a semi-flexible structure with three layers, including inner rubber layer, steel sheet layer and outer rubber layer. The inflatable pressure is applied on the surface of the inner rubber layer, and the tool offset is applied by moving the workpiece. The simulated parameters are shown in Tab. 1.The detailed modeling method can be found in our previous research [8,9]. The simulated contact pressure is shown in Fig. 4.

Table 1. Simulated parameters

Workpiece type	H (mm)	R_1 (mm)	ρ (°)	Pressure (MPa)
Convex R_c=2500\2000\1500\1000\500\250	0.6\0.8\1\1.2	80	23	0.1
Plane				
Concave R_c=2500\2000\1500\1000\500\250				

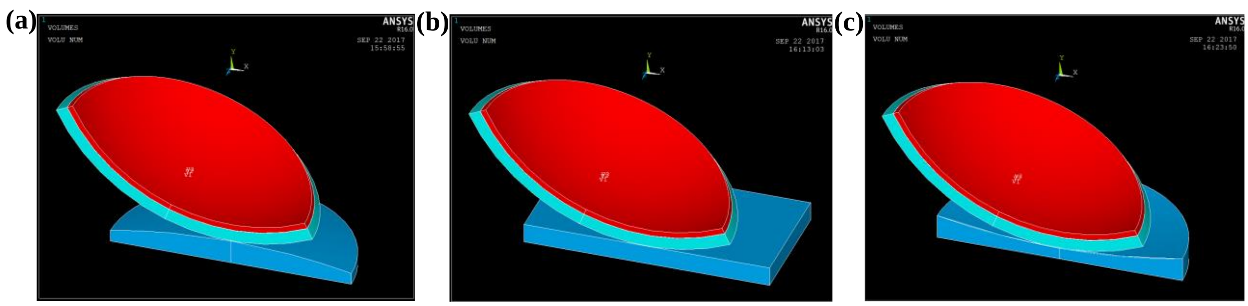

Fig. 3. ANSYS analysis model. (a) Convex surface, (b) plane surface, (c) concave surface.

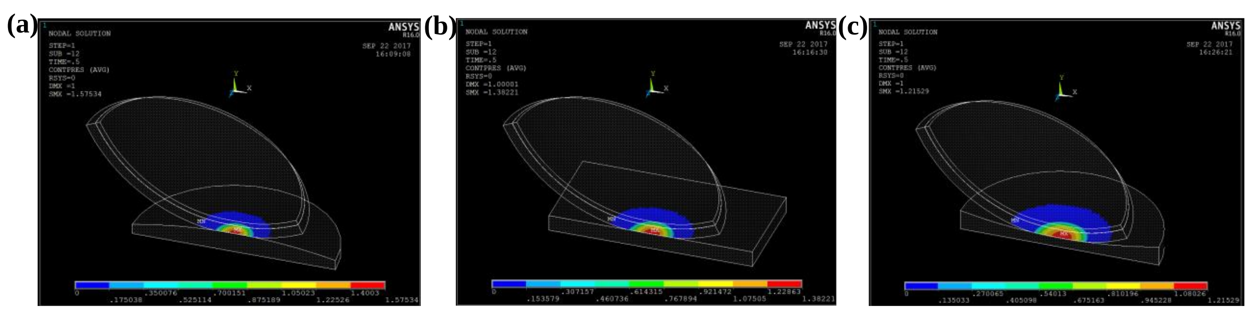

Fig. 4. Contact pressure. (a) Convex surface, (b) plane surface, (c) concave surface.

The contact pressure between the bonnet and the workpiece was fitted using the Hertz equation, which is

$$P = A\left(1 - \frac{X^2}{B^2} - \frac{Y^2}{C^2}\right)^m \qquad \textbf{(3)}$$

where m denotes the shape factor, whose value is 1, A denotes the maximum contact pressure value in the contact area, B and C denote the half-length and half-width of the elliptical contact area.

Hertz equation is performed on fitting the pressure distribution to determine the fitting coefficients (A\$B$\$C$) under different simulation parameters. In order to ensure the fitting accuracy, the root mean square (*RMSE*) of the error between the fitting data and the original data is better than 0.05. The fitting coefficients under different parameters are shown in Tab. 2.

Table 2. The fitting coefficients ($A\backslash B\backslash C$) related to the curvature radius R and the compression H

Workpiece type	radius R_c	Fitting coefficient A				Fitting coefficient B				Fitting coefficient C			
		Compression H (mm)				Compression H (mm)				Compression H (mm)			
		0.6	0.8	1	1.2	0.6	0.8	1	1.2	0.6	0.8	1	1.2
Convex	500	1.034	1.295	1.485	1.598	8.324	9.572	10.730	11.820	8.309	9.625	10.920	12.280
	1000	1.017	1.273	1.462	1.551	8.631	9.9140	11.160	12.340	8.619	10.020	11.390	12.810
	1500	1.009	1.263	1.444	1.536	8.740	10.040	11.300	12.520	8.737	10.170	11.560	13.030
	2000	1.006	1.26	1.444	1.527	8.804	10.100	11.390	12.620	8.797	10.250	11.650	13.140
	2500	1.002	1.256	1.441	1.523	8.860	10.140	11.430	12.680	8.828	10.290	11.700	13.200
Plane	/	0.989	1.245	1.424	1.503	9.020	10.320	11.620	12.920	8.976	10.480	11.920	13.440
Concave	-2500	1.034	1.23	1.404	1.486	9.167	10.520	11.820	13.170	9.143	10.660	12.140	13.700
	-2000	1.017	1.221	1.400	1.482	9.197	10.570	11.870	13.230	9.186	10.700	12.200	13.770
	-1500	1.009	1.217	1.391	1.474	9.258	10.820	11.990	13.340	9.255	10.950	12.330	13.890
	-1000	1.006	1.213	1.383	1.459	9.400	10.820	12.190	13.570	9.399	10.960	12.520	14.100
	-500	1.002	1.182	1.352	1.409	9.825	11.360	12.840	14.340	9.880	11.540	13.200	14.930

Then, the least square method with binary quadratic equations was used to obtain the analytical expressions of the fitting coefficients ($A\backslash B\backslash C$) related to the R_c and the H. In order to ensure the fitting accuracy, *RMSE* is better than 0.015. According to Tab.2, the analytical expressions of the fitting coefficients ($A\backslash B\backslash C$) related to R_c and H can be obtained. Finally, the mathematical expressions of the contact pressure P about the curvature radius R_c and the compression H can be obtained:

$$\begin{cases} P = A(1-\dfrac{X^2}{B^2}-\dfrac{Y^2}{C^2}) \\ A = -0.2421-4.22E\text{-}5\cdot R_c+2.785\cdot H+1.6E\text{-}8\cdot R_c^2 \\ \quad -3.12E\text{-}5\cdot R_c\cdot H-1.025\cdot H^2 \\ B = 4.053+7.31E\text{-}4\cdot R_c+6.808\cdot H-2.18E\text{-}7\cdot R_c^2 \\ \quad +2.57E\text{-}4\cdot R_c\cdot H-0.5463\cdot H^2 \\ C = 4.092+7.79E\text{-}4\cdot R_c+6.175\cdot H-2.4E\text{-}7\cdot R_c^2 \\ \quad +3.12E\text{-}4\cdot R_c\cdot H+0.2187\cdot H^2 \end{cases} \tag{4}$$

$$\begin{cases} P = A(1-\dfrac{X^2}{B^2}-\dfrac{Y^2}{C^2}) \\ A = -0.01187+3.01E\text{-}5\cdot R_c+2.095\cdot H-1.18E\text{-}8\cdot R_c^2 \\ \quad +3.23E\text{-}5\cdot R_c\cdot H-0.7688\cdot H^2 \\ B = 5.625-1.02E\text{-}3\cdot R_c+8.172\cdot H-3.16E\text{-}7\cdot R_c^2 \\ \quad -3.91E\text{-}4\cdot R_c\cdot H-0.3788\cdot H^2 \\ C = 5.512-1.09E\text{-}3\cdot R_c+8.151\cdot H+3.31E\text{-}7\cdot R_c^2 \\ \quad -3.94E\text{-}4\cdot R_c\cdot H+0.1537\cdot H^2 \end{cases} \tag{5}$$

Equations (4) and (5) are the contact pressure expressions of the bonnet-convex surface and the bonnet-concave surface, respectively.

B. Velocity distribution by kinematic analysis

Fig. 5 shows the geometric model of the contact between the bonnet and the convex surface. R_1 is the bonnet radius, R_c is the workpiece radius, H is the compression, h is the height of the workpiece in the contact area, r is the radius of the contact area, and O is the bonnet center. O_1 is the intersection of the spindle axis and the contact interface, and ω is the spindle speed. O_2 is the center of the contact area, which is the origin of the coordinate system XYZ. p is an arbitrary point on the workpiece surface in the contact area, whose coordinate is (x_p, y_p, z_p), and p_1 is the projection of point p on the axis of the bonnet spindle.

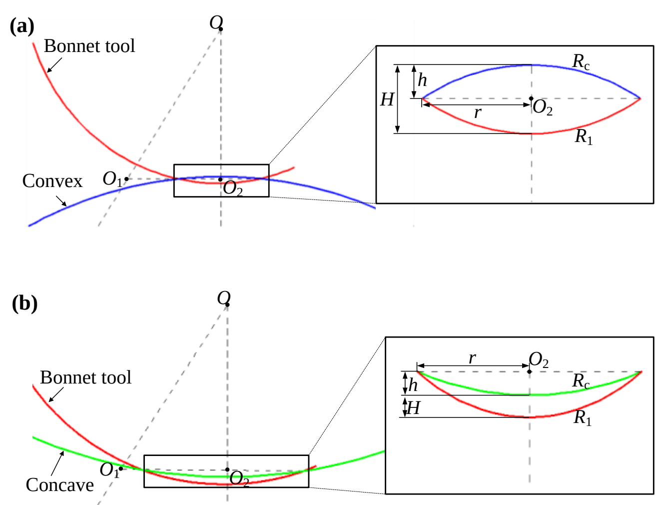

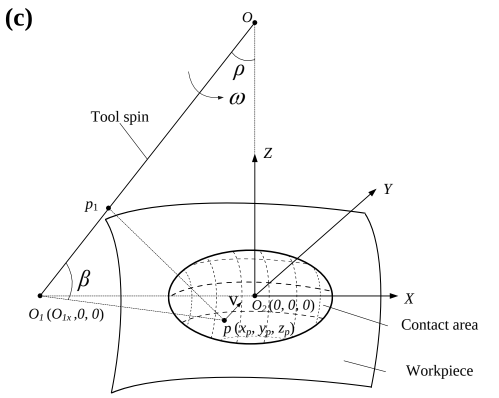

Fig. 5. The geometric model of the contact between the bonnet and the spherical surface. (a) Two-dimensional model between bonnet and convex sphere, (b) Two-dimensional model, (c) Three-dimensional model.

According to the two-dimensional model of the contact between the bonnet and the convex surface shown in Fig. 5(a), the coordinates of the contact point on the convex surface in the coordinate system *XYZ* can be derived by equations (6)-(8):

$$h = (2R_1H - H^2)/2(R_1 + R_c - H) \quad \textbf{(6)}$$

$$r = sqrt(2R_ch - h^2) \quad \textbf{(7)}$$

$$\begin{cases} z(x,y) = sqrt(R_2{}^2 - x^2 - y^2) - R_c + h \\ x, y \in [-r, r] \quad (x^2 + y^2) \in [0, r] \end{cases} \quad \textbf{(8)}$$

According to the two-dimensional model of the contact between the bonnet and the concave surface shown in Fig. 5(b), the coordinates of the contact point on the concave surface in the coordinate system *XYZ* can be derived by equations (9) -(11):

$$h = (2R_1H - H^2)/2(R_c - R_1 + H) \quad \textbf{(9)}$$

$$r = sqrt(2R_ch - h^2) \quad \textbf{(10)}$$

$$\begin{cases} z(x,y) = -\left[sqrt(R_c{}^2 - x^2 - y^2) - R_c + h\right] \\ x, y \in [-r, r] \quad (x^2 + y^2) \in [0, r] \end{cases} \quad \textbf{(11)}$$

According to the three-dimensional model of the contact between the bonnet and the spherical surface shown in Fig. 5(c), the velocity distribution of the contact area in the coordinate system *XYZ* can be derived:

$$\begin{cases} |Op| = sqrt(x_p{}^2 + y_p{}^2 + (z_p - z_o)^2) \\ |O_1p| = sqrt((x_p - x_{o_1})^2 + y_p{}^2 + z_p{}^2) \\ |O_1O| = sqrt(x_{o_1}{}^2 + z_o{}^2) \\ \beta = a\cos\left[(|Op|^2 + |O_1p|^2 - |O_1O|^2)/(2|O_1p||O_1O|)\right] \\ V = 2\pi\omega|O_1p|\sin\beta \end{cases} \quad \textbf{(12)}$$

Substituting equations (6) - (8) into equation (12) can obtain the velocity distribution *V* of the contact area between the bonnet and the convex surface. Similarly, substituting equations (9) - (11) into equation (12) , the velocity distribution *V* of the contact area between the bonnet and the concave surface can be obtained.

C. TIF Related to Curvature and Simulation

The removal distribution R_{TIF} can then be obtained based on the pressure distribution *P* and the velocity distribution *V*. Fig. 6 shows the TIF of the bonnet contacting with different radius spheres under conditions of 1mm bonnet compression, 100 rpm rotation speed, 1 min polishing time, and the value of the Preston coefficient *K* was 1.

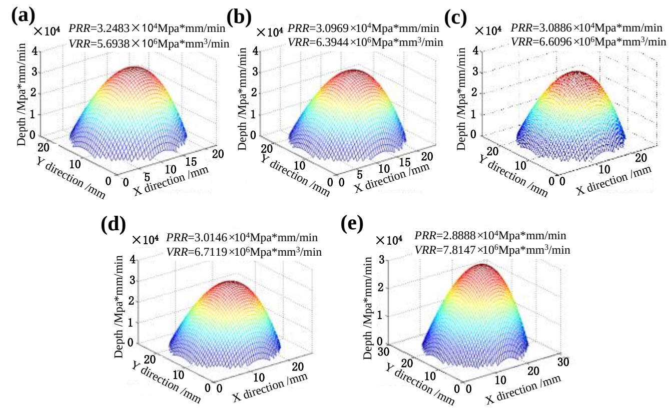

Fig. 6. TIFs of the bonnet contacting with different radius spheres. (a) R_c=250 convex, (b) R_c=2500 convex, (c) plane, (d) R_c=2500 concave, (e) R_c =250 concave.

In Fig. 6, *PRR* is the peak removal rate and *VRR* is the volume removal rate. When the workpiece is a convex surface, larger curvature radius leads to smaller *PRR* and larger *VRR*. When the workpiece is a concave surface, larger curvature radius leads to the larger *PRR* and smaller *VRR*.

3.2. Establishment of the time-varying TIF model related to the processing position of aspheric surface

The curvature parameter R_c in the TIF model related to the workpiece curvature is related to the polar distance D_p. In addition, the D_p is related to the processing point position, which is determined by the path and polishing time. In the case of a aspheric surface, when the geometrical center of the aspheric surface is used as the coordinate origin, the D_p of the position (x, y) is:

$$D_p = sqrt\left[(D_x + x)^2 + \left(D_y + y\right)^2\right] \quad \textbf{(13)}$$

where D_x is the distance between the polar center and the geometrical center of the aspheric surface in the X direction, D_y is the distance between the polar center and the geometrical center of the aspheric surface in the Y direction.When $D_x = 0$ and $D_y = 0$, the aspheric surface is rotationally symmetric. Besides, it is off-axis aspherical.

In Eq. (10), the coordinates (x, y) of the polishing tool on the aspheric surface can be considered as a function related to the polishing time:

$$x = f_x(t)\ ,\ y = f_y(t) \quad \textbf{(14)}$$

Substituting equations (10), (11), and (1) into equation (2), a time-varying TIF model related to the processing position (or processing time) of aspheric surface can be obtained.

$$R_{TIF}(t) = \frac{1}{T}\int_0^T K \cdot P\left\{f_{Rc}[f_x(t)^2 + f_y(t)^2]\right\} \cdot V\left\{f_{Rc}[f_x(t)^2 + f_y(t)^2]\right\}dt \quad \textbf{(15)}$$

Fig. 7 is the calculation flow of the time-varying TIF for the large aspheric elements.

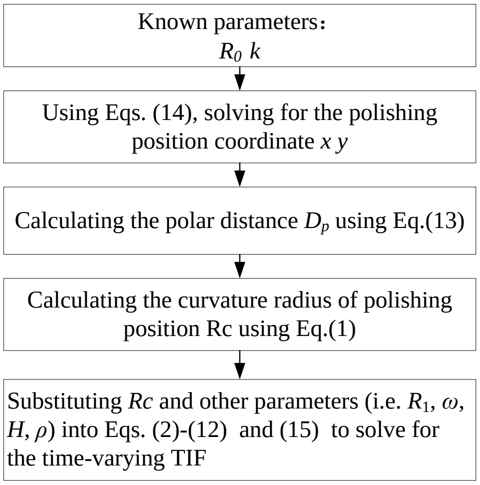

Fig. 7. Calculating flow for the time-varying TIF.

4. EXPERIMENTAL VALIDATION AND DISCUSSION

In order to verify the correctness of the above model, the spot experiment with different curvature workpieces were carried out, as shown in Fig. 8 (a). The removal processes are conducted on three Φ150mm sio_2 glasses (i.e. a convex, a plane and a concave), the peak values (PVs) of which are pre-polished to ~0.15um. Besides, on each workpieces, four spots are obtained to make sure the correctness of the results. Other experimental conditions are listed in Tab. 3. After the polishing process, the spots are measured by a QED made interferometer with model ASI(Q), as shown in Fig. 8 (b).

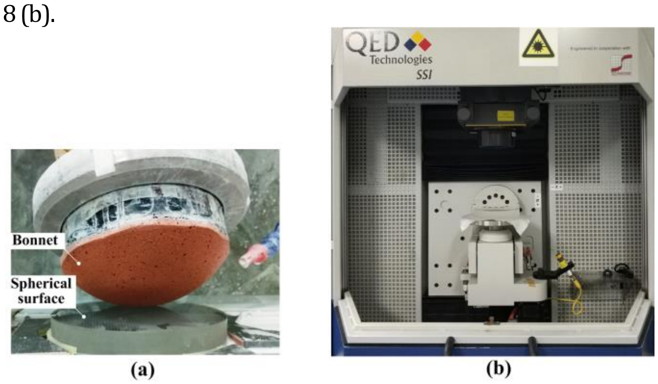

Fig. 8. The experimental pictures. (a) the machining picture and (b) the measuring picture.

In the Preston formula, the Preston coefficient K is used to characterize the effect of factors other than velocity and pressure on the removal efficiency. K is a constant, and its value can be calculated based on experimental and simulation results. In order to make the actual TIF coincide with the theoretical TIF better, the coefficient K_i at point i of the TIF is solved, and the average value of K_i is taken as the comprehensive coefficient K.

$$\begin{cases} K_i = Z_{actual\text{-}i} / (V_i * P_i) \\ K = \sum_{i=1}^{n} K_i / n \end{cases} \quad \textbf{(16)}$$

where Z_{actual} is the experimental TIF, V is the simulated velocity distribution and the P is the simulated pressure distribution.

According to the parameters listed in Tab. 3, the actual TIF was obtained experimentally. Fig. 9 reveals polishing spots with different curvature workpieces. The velocity and pressure in the polishing area were obtained based on the theoretical analysis. The K is 6.3×10^{-6} calculated by the formula (13). The simulated TIFs of the bonnet contacting with different curvature workpieces were compared with the experimental TIFs as shown in Fig. 10.

Table 3. Simulated parameters

Workpiece type	R_1 (mm)	Bonnet rev (rpm)	H (mm)	Pressure (MPa)	ρ (°)	T (s)
Convex R_c=500	80	500	0.6	0.1	23	6
Plane						
Concave R_c=500						

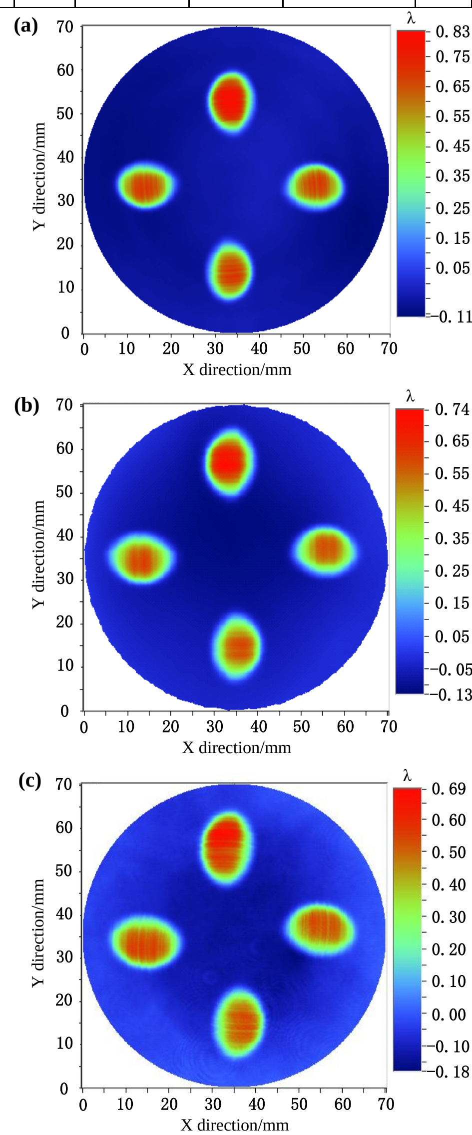

Fig. 9. TIFs with different curvature workpieces. (a) convex R_c=500, (b) plane, (c) concave R_c=500.

Table 4. Comparison between experimental results and theoretical results

Workpiece type	Experimental results								Theoretical results	
	Peak removal rate (λ/s)				Volume removal rate (mm³/min)				Peak removal rate (λ/s)	Volume removal rate (mm³/min)
Convex R_c=500	0.15	0.13	0.14	0.13	0.48	0.42	0.44	0.41	0.110	0.450
Plane	0.14	0.12	0.12	0.11	0.52	0.43	0.46	0.43	0.106	0.505
Concave R_c=500	0.13	0.12	0.12	0.11	0.62	0.55	0.56	0.52	0.106	0.608

Fig. 10 shows that removal rate has the same variation tendency to the curvature radius of in simulation and experiment. Workpiece curvature has little effect on peak removal rate, but has a significant effect on volume removal rate. As shown in Tab. 4 and Fig. 10, the deviations of peak removal rate of TIF on convex, plane and concave are 20.0%, 13.3% and 11.5%, respectively. And the deviations of volume removal rates between them are 2.8%, 9.8% and 8.0%, respectively. The experimental results exhibited good agreement with the theoretical results on the volume removal rate, which verified the effectiveness and correctness of the proposed model. However, it is necessary to point out that the possible reason of the bigger deviation of peak removal rate between experimental and simulated results is that the peak removal rate is more susceptible to the instability of polishing conditions, i.e., polishing fluid, tool condition and polishing environment in the actual polishing process.

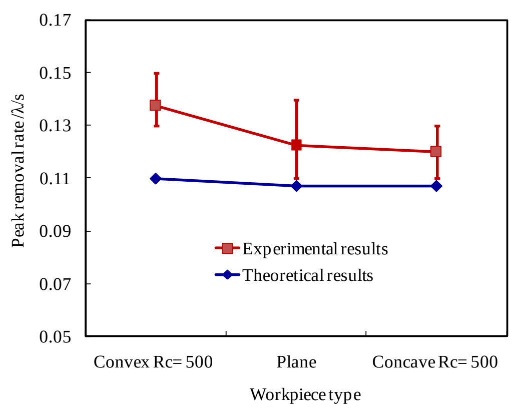

(a)

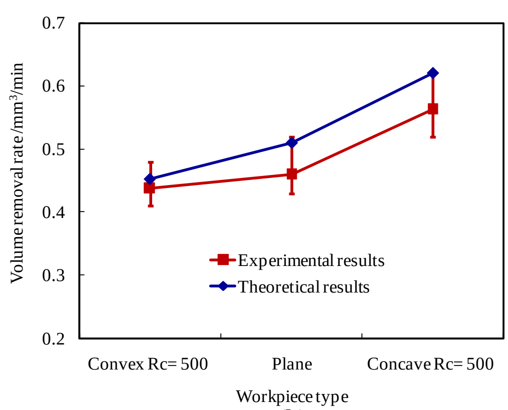

(b)

Fig. 10. Comparison of experimental and simulated TIF' removal rate. (a) peak removal rate, (b) volume removal rate.

5. CONCLUSIONS

A novel time-varying TIF modeling method considering the curvature effect during bonnet polishing on aspheric surface was proposed in this paper. Both simulation and experiments were conducted to verify the effectiveness of this method. And the deviations of TIF with respect to volume removal rate between the simulation and experimental results were less than 10%, which validates of the proposed model. This model will provide a theoretical foundation to compensate the dynamic error induced by the curvature effect during bonnet polishing on aspheric surface. Moreover, this method is also suitable for the TIF prediction of bonnet polishing on the freeform surfaces.

Funding Information. This work was financially supported by the Science Challenge Project (No. JCKY2016212A506-0502) and the Youth Talent Fund of Laser Fusion Research Center, CAEP. (No. RCFCZ1-2017-6).

Acknowledgment. We appreciate the invaluable expert comments and advice on the manuscript from all anonymous reviewers.

References

1. D. D. Walker, D. Brooks, A. King, R. Freeman, R. Morton, G. McCavana, S. W. Kim. "The 'Precessions' tooling for polishing and figuring flat, spherical and aspheric surfaces," Optics Express. 11(8), 958-64 (2003).
2. A. Beaucamp, Y. Namba, P. Charlton. "Corrective finishing of extreme ultraviolet photomask blanks by precessed bonnet polisher," Applied Optics, 53(14),3075-3080 (2014).
3. A. Beaucamp, Y. Namba. "Super-smooth finishing of diamond turned hard X-ray molding dies by combined fluid jet and bonnet polishing," CIRP Annals-Manufacturing Technology. 62(1),315-8 (2013).
4. C. Wang, Z. Wang, Q. Wang, X. Ke, B. Zhong, Y. Guo, Q. Xu. "Improved semirigid bonnet tool for high-efficiency polishing on large aspheric optics," The International Journal of Advanced Manufacturing Technology, 88(5-8), 1607-1617(2017).
5. C. Wang, W. Yang, Z. Wang, X. Yang, C. Hu, B. Zhong, Y. Guo, Q. Xu. "Dwell-time algorithm for polishing large optics," Applied optics, 53(21), 4752-4760 (2014).
6. D. W. Kim and S. W. Kim. "Static tool influence function for fabrication simulation of hexagonal mirror segments for extremely large telescopes," Optics Express, 13(3), 910-917(2005).
7. H. Y. Li, D. D. Walker, G. Y. Yu, and W. Zhang. "Modeling and validation of polishing tool influence functions for manufacturing segments for an extremely large telescope,"Applied Optics, 52(23), 5781-5787(2013).
8. C. Wang, Z. Wang, X. Yang, Z. Sun, Y. Peng, Y. Guo, and Q. Xu. "Modeling of the static tool influence function of bonnet polishing based on FEA," The International Journal of Advanced Manufacturing Technology, 74(1-4), 341-349(2014).
9. X. L. Ke, C. J. Wang, Y. B. Guo, Q. Xu. "Modeling of tool influence function for high-efficiency polishing," The International Journal of Advanced Manufacturing Technology, 84(9-12), 2479-2489 (2016).

10. S. Zeng, L. Blunt. "Experimental investigation and analytical modeling of the effects of process parameters on material removal rate for bonnet polishing of cobalt chrome alloy," Precision Engineering, 38, 348-355 (2014).
11. Z. C. Cao, F. C. Chi, Z. Xing. "A theoretical and experimental investigation of material removal characteristics and surface generation in bonnet polishing," Wear, 360, 137-146 (2016).
12. R. Pan, B. Zhong, D. Chen, Z. Wang, J. Fan, C. Zhang, and S. Wei, "Modification of tool influence function of bonnet polishing based on interfacial friction coefficient," International Journal of Machine Tools and Manufacture, 124, 43-52 (2018).
13. S. Wan, X. Zhang, H. Zhang, M. Xu, X. Jiang. "Modeling and analysis of sub-aperture tool influence functions for polishing curved surfaces," Precision Engineering, 51,415-25 (2018).
14. J. F. Song, Y. X. Yao, Y. G. Dong, B. Dong. "Prediction of surface quality considering the influence of the curvature radius for polishing of a free-form surface based on local shapes," The International Journal of Advanced Manufacturing Technology, 95 (1), 1-15 (2017).
15. X. H. Chen, B. Zhong, J. Wang, et al. "Distortion of removal function based on the local asphericity of aspheric surface and the viscoelasticity of polishing tool in computer-controlled optical surfacing," Part C: J Mechanical Engineering Science, 232(7), 1135-1145 (2018).